

# PATCH-BASED SEGMENTATION OF OVERLAPPING CERVICAL CELLS USING ACTIVE CONTOUR WITH LOCAL EDGE INFORMATION

*Alaa Khadidos, Victor Sanchez and Chang-Tsun Li*

Department of Computer Science, University of Warwick, UK

## ABSTRACT

The Pap test is a manual screening procedure that is used to detect the precursor lesions of cervical cancer by analyzing changes in nuclei and cytoplasm of cervical cells. Due to the sensitivity of the Pap test to intra- and inter-observer variability, automating the procedure using digital image analysis test is still an open problem. Within this context, segmentation of overlapping cervical cells is a key component to develop image analysis methods. In this paper, we propose a framework for segmenting the cytoplasm of each individual cell depicted within an image of overlapping cervical cells. The proposed framework uses a patch-based approach where a parametric active contour detects, on a patch-by-path basis, the cytoplasm boundary of each overlapping cell. The active contour within the patch deforms under the influence of Gradient Vector Flow (GVF) forces computed based on the local edges depicted in each patch region. Results show that the proposed framework achieves more accurate cytoplasm segmentation results compared to the current state-of-art methods.

**Index Terms**— Active contours, overlapping cervical cells, Pap test, patch-based segmentation, Gradient Vector Flow (GVF)

## 1. INTRODUCTION

Cervical cancer is one of the most common types of cancer among women [1]. Since the introduction of the Pap test, a significant decrease has been observed in the incidence of cervical cancer and related deaths. The Pap test, which has been one of the most effective cancer screening tests, remains the most important technique in detecting the precursor lesions of cervical cancer. The test is based on obtaining cells from the uterine cervix and then smearing them onto glass slides for microscopic examination to detect human papillomavirus's (HPV's) effects. The Papanicolaou (Pap) method is then used to stain the slides, which makes analysis easier as different components of the cells show different colours. The sensitivity of the Pap test can be affected mainly by the number of cells sampled, the overlap among them, the poor contrast of the cell cytoplasm, and the presence of mucus, blood cells, and inflammatory cells [2]. Both intra- and inter-observer variability during the interpretation of abnormal smears contribute to the wide variation in false-negative results [3]. In order to tackle these issues, techniques for cell deposition have been improved. Cell deposition techniques purify cells from a significant portion of blood, mucus, and other debris. Also, they reduce the overlap among cells increasing the likelihood of cells occurring on a single focal plane. [4].

The difficulties associated with manual screening and the promise of early diagnosis have increased the interest on systems capable of capturing digital images by connecting digital cameras to microscopes. The resulting digital images can then be used to develop automated and semi-automated image analysis techniques, which tend to be more robust and consistent than manual analysis.

These image analysis systems also facilitate a more quantifiable examination of the smears, which has the potential of increasing the reliability of the diagnoses [5, 6].

Automated and semi-automated image analysis techniques improve both the sensitivity and specificity of screening, which involves two main tasks: segmentation and classification. Segmentation tasks mainly focus on detecting and segmenting cells boundaries, separating them from the background, as well as detecting and segmenting the corresponding nuclei. Automatic thresholding, morphological operations, and active contour models are the most popular approaches for biomedical image segmentation [2, 7, 8, 9]. Classification tasks, on the other hand, focus on classifying individual cells using, for example, a number of features such as texture, pixel intensities and shape [10, 11, 12, 13, 14].

Several authors have proposed methods to detect and segment the nucleus of cervical cells. For example, Plissiti et al. [15] propose an automated method for the detection and boundary determination of cervical cell nuclei. This method uses a marker-based watershed segmentation approach to first find the nucleus boundaries. It then eliminates false-positive regions by using a binary classifier with shape, texture, and intensity features. Despite its potential, this method only focuses on the segmentation of nuclei, which tend to be depicted with relatively high contrast around the boundaries, and are thus, easier to segment than cytoplasm.

As the cytoplasm features have been shown to be very useful for the identification of abnormal cells, the detection of the cytoplasm regions from isolated cervical cells is also crucial [16]. For example, Li et al. [12] propose a method using  $k$ -means clustering with three classes to identify nuclei, cytoplasm, and background regions. They employ snake active contours to refine the nucleus and cytoplasm boundaries.

Other more recent approaches focus on the individual segmentation of cytoplasm and their corresponding nuclei on images depicting overlapping cells. Lu et al. [17, 2] propose a method that employs a joint optimization of multi-level set functions constrained by the length, area and shape of cells. The method first detects cell clumps and all nuclei within those clumps. It then employs several levels set functions for each cell within a clump. These levels set functions interact with each other using both unary (intra-cell) and pairwise (inter-cell) energy terms. Nosrati et al. [18] propose a continuous variational segmentation framework using directional derivatives to segment overlapping cervical cells by incorporating a star-shape-prior within a level set method.

This paper proposes a framework for individual segmentation of overlapping cytoplasm in cervical cells images. The proposed framework, which is also capable of detecting the corresponding nuclei, first employs a supervised classifier to separate cell clumps from the background. It then employs a patch-based approach where parametric active contours detect, on a patch-by-path basis, the cytoplasm boundary of each overlapping cell in a cell clump. The active

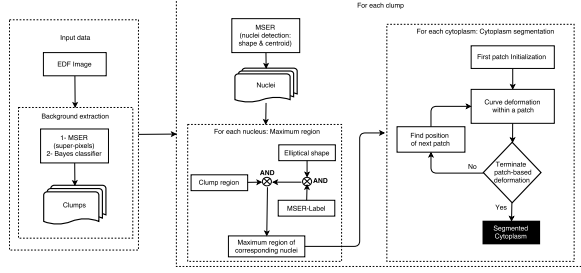


**Fig. 1.** Overview of the proposed framework. The background extraction stage aims at separating all cell clumps from the background, and identifying the maximum region of each individual cytoplasm within each cell clump. The cytoplasm segmentation stage aims at segmenting the cytoplasm of each cell within each clump.

contour within each patch deforms under the external influence of Gradient Vector Flow (GVF) forces computed based on the local edges depicted in each patch region. The framework is evaluated on real Extended Depth Field (EDF) images, and compared against the state-of-the-art methods in [19, 2]. Results show that the proposed framework leads to more accurate cytoplasm segmentation results compared to the current state-of-art methods.

The rest of the paper is organized as follows. Our proposed framework is detailed in Section 2. Experimental results are presented in Section 3. Finally, Section 4 concludes this paper.

## 2. PROPOSED FRAMEWORK

For each EDF image, which are obtained as detailed in [20], our framework performs the segmentation of overlapping cervical cells in two main steps. The first step consists of the segmentation of clumps, detection of all nuclei in each clump using the Maximally Stable Extremal Regions (MSEr) algorithm [21], and identification of the maximum region of each cell within each clump. The second step focuses on cytoplasm segmentation for each cell within each clump. A diagram of the proposed framework illustrating the constituent stages is shown in Fig. 1. We explain each stage next.

**Background extraction.** This stage aims at dividing the EDF image into cell and background regions. Cell regions correspond to the regions containing overlapping cervical cells, the so-called cell clumps, while background regions correspond to the remaining empty area. This stage reduces the search space for the subsequent stages by concentrating on cell clumps. Cell clumps, which may include overlapping cells or isolated cells, are detected as follows. The quick shift algorithm [22] is first applied to find local maxima of a density function that takes into account pixel value similarities and spatial proximity between pixels and the centroids of clusters. The outcome of this process is a map of super-pixels,  $Q_S$ , in which super-pixels are labelled with values in the range  $[0, 1]$ , as exemplified in Fig. 2(b). A naive Bayes classifier is then run on map  $Q_S$  with two classes, cell clumps and background. This classifier results in a binary image that is used as a mask, denoted by  $B$ , that indicates the position of clumps [see Fig. 2 (c)].

**Detection of nuclei in each clump.** Nuclei are usually characterized by relatively low gray values, homogeneous textures, and well-defined (almost circular) boundaries. Based on the assumption that nuclei do not overlap and that each nucleus represents one cell, the MSEr algorithm is used to detect stably connected components. These components are characterized by blobs that represent the candidate nuclei. Some of these candidates are filtered out if their sizes

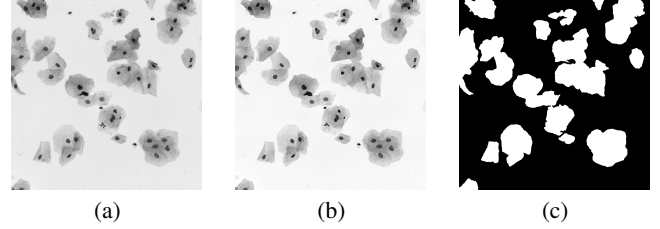


**Fig. 2.** (a) Example of an extended depth field (EDF) cervical cytology image. (b) Corresponding over-segmented super-pixel map generated by quick shift ( $Q_S$ ). (c) Corresponding binary image representing cell clumps produces by a Bayes classifier.

are not within specific threshold range. In our experiments, the size of the blob should be within the range  $\in [200, 600]$  pixels, as the majority of nuclei in cervical cell images have a size within this range.

**Cell Segmentation.** Based on our observations, cytoplasm boundaries are usually located at the same radial distance from the centroid of their associated nucleus. To segment a cell, the maximum possible region of each cytoplasm in the clump is first found based on the orientation of the corresponding nucleus. This is based on the observation that the orientation of the nucleus is a good estimator of the orientation of its cytoplasm. Therefore, the geometry of each detected nucleus is used to define an ellipse that represents the maximum region of the corresponding cytoplasm. Specifically, this maximum region is defined as an ellipse with the same orientation as the ellipse bounding the nucleus, but with a major axis equal to the distance between the current nucleus and the closest neighboring nucleus. The minor axis of this ellipse is then adjusted to ensure that the orientation of the ellipse matches the orientation of the nucleus. We denote this ellipse by  $E_{ellipse}$ . The maximum region of each cell is then given by:

$$CM = OB \wedge B \quad (1)$$

where  $OB = Q_L \cap E_{ellipse}$ , and  $Q_L$  is the label map produced by quick shift. An example  $Q_L$  is shown in Fig. 3 (a), where each super-pixel is shown using a different color. The black contour in Fig. 3 (a) represents the outer border of all regions in  $Q_L$  that overlap  $E_{ellipse}$ , i.e., the outer border of  $OB$ .  $E_{ellipse}$  is shown as a white contour in the figure. The outer contour of  $OB$  is used to define  $CM$  by using information from binary mask  $B$ . This is depicted Fig. 3 (b) as a red contour. Points  $L_0$  and  $L_1$  in Fig. 3 (c) represent possible positions for patch initialization. The path-based deformation is run to detect the section of the cytoplasm boundary that overlaps other cells, which is denoted by  $Cell_{overlap}$ . This is depicted in red in Fig. 3 (c). Note that the section of the cytoplasm boundary that does not overlap other cells, depicted in blue in Fig. 3 (c), is easily identified by computing the outer boundary of the cell clump and the maximum region of each individual cell. We denote this section by  $Cell_{noOverlap}$ .

**Patch-based deformation.** Let  $P_0$  be an initial square patch of size  $\tau \times \tau$  pixels and centred at  $L_0$  (or  $L_1$ ). This is illustrated in Fig. 4. Inside this initial patch, an open curve  $C_{P_0}(s) = [x(s), y(s)]$ ,  $s \in [0, 1]$  is initialized, which represents a parametric active contour. Curve  $C_{P_0}(s)$  is perpendicular to the line connecting the centroid of the nucleus, denoted by  $c$ , and the centroid of the patch  $m$ , denoted by  $c_m$  [see Fig. 4(b)]. For each cell,  $Cell_{overlap}$  is computed as follows:

$$Cell_{overlap} = E_{patch}(C_{P_0}) \cup E_{patch}(C_{P_1}) \cup E_{patch}(C_{P_2}) \cup \dots \cup E_{patch}(C_{P_M}) \quad (2)$$

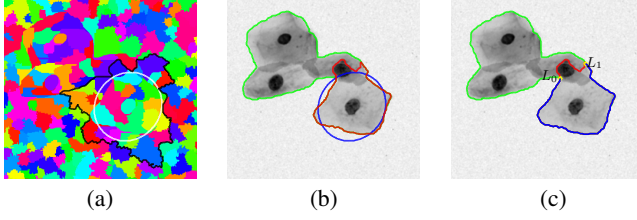


**Fig. 3.** (a) Example of a labelled map generated by quick shift ( $Q_L$ ); the white contour denotes an example  $E_{ellipse}$ , and the black contour denotes the outer border of all regions that overlap  $E_{ellipse}$ . (b) The green contour denotes the clump border and the red contour denotes the maximum region of the cell. (c) The yellow stars denote  $L_0$  and  $L_1$ , the possible positions for patch initialization

where  $M$  represents the total number of required patches to segment  $Cell_{overlap}$ , and  $E_{patch}(C_{P_m})$  is an energy function to be minimized for curve  $C_{P_m}(s)$  in patch  $m$ . Patch  $P_{m+1}$  is defined as patch  $P_m$ ; however,  $P_{m+1}$  is initialized based on the results of the deformable open curve from patch  $P_m$ , where the last element from the curve in patch  $P_m$  is the centroid of patch  $m+1$ ; i.e.,  $c_{m+1}$ . In order to perform the operation in Eq. (2), the result of deforming the open curve in each patch is taken as the section of the curve within the region of patch that does not overlap the adjacent patch. The final cytoplasm boundary is just the union of  $Cell_{overlap}$  with  $Cell_{noOverlap}$ . It is important to mention that the reason for the initial open curve within patch  $P_m$  to be defined as being perpendicular to the line connecting  $c$  and  $c_m$  is to provide circular motion of patches around the nucleus.

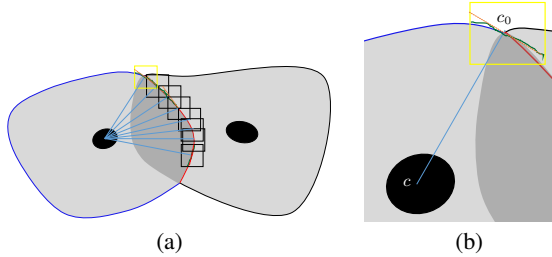


**Fig. 4.** (a) Example synthetic overlapping cells; the red contour denotes  $Cell_{noOverlap}$ , the yellow rectangle denotes patch  $P_0$ , and the black rectangles denote the subsequent patches. (b) A close-up view of patch  $P_0$ ; the orange dotted line denotes the initial open curve, which is perpendicular to the light blue line connecting  $c$  and  $c_0$ ; the green contour denotes the result of the deformable curve for this patch.

The open curve that is initialized in patch  $P_m$  evolves to the object's boundary within the patch by minimizing the following energy function:

$$E_{patch}(C_{P_m}) = \frac{1}{2} \int_0^1 (\alpha |C'_{P_m}(s)|^2 + \beta |C''_{P_m}(s)|^2) ds + \int_0^1 E_{ext}(C_{P_m}(s)) ds \quad (3)$$

where  $\alpha$  and  $\beta$  are weighting parameters that control the curve's tension and rigidity, respectively. The first integrand in Eq. (3) is referred to as the internal energy, which controls the smoothness of  $C_{P_m}$ , while the second integrand is referred to as the external energy [i.e.,  $E_{ext}(C_{P_m}(s))$ ], which attracts  $C_{P_m}$  towards the object's

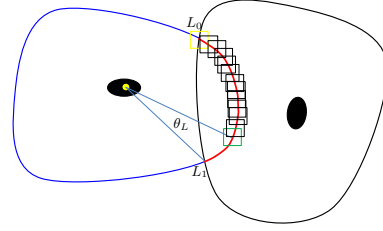


**Fig. 5.** Example of synthetic overlapping cells; the red contour is the section of the cytoplasm boundary detected by the proposed patch-based deformation; the yellow rectangle denotes patch  $P_0$ , the black rectangles denote the subsequent patches and the green rectangle denotes the last patch. i.e., patch  $P_M$ .

boundary; in this case, to the section of the cytoplasm's boundary depicted within the patch.

The external energy consists of GVF forces [9], which employ an edge map computed using a Canny edge detector. GVF forces are computed for each patch and thus, change according to the edges depicted within the patch. Performing the deformation on a patch-by-patch basis provides two main advantages. First, the overall computational cost is reduced as the deformation is performed only on the patches, not the whole image. Second, computing the GVF on each patch provides more precise local edge features than those obtained by computing the GVF over the whole image, where small edge features may be neglected.

The minimization of  $E_{patch}(C_{P_m})$  can be achieved by evolving the curve dynamically as a function of parameter  $s$  and artificial time  $t$  as follows:

$$C_{P_m}(s, t) = [\alpha C''(s, t) - \beta C''''(s, t)] - \nabla E_{ext} \quad (4)$$

where the first term and the second term are called the internal force and the external force, respectively, and  $\nabla$  denotes the gradient operator performed on GVF forces. It is important to mention that detecting the maximum region of a cell helps limiting the final cytoplasm boundary to this maximum region, as patches are always initialized within this maximum region.

**Termination of patch-based deformation.** The patch-based deformation is terminated if the angle between the line connecting  $c$  and  $c_m$  and the line connecting  $c$  and  $L_1$  (i.e., the other end of  $Cell_{noOverlap}$ ) is less than  $\theta_L$ . This is illustrated in Fig. 5. To refine the final contour that represents the cell cytoplasm, a live-wire algorithm [23] is applied between points  $c_M$  and  $L_1$ .

### 3. PERFORMANCE EVALUATION

In this paper we used a subset of five real EDF images, as tested in [2]. Each image in this dataset has up to 15 clumps and each clump contains a varying number of cells with an overlap coefficient in the range  $\in [0.0, 0.9]$ , 0.0 indicates no overlap while 0.9 indicates 90% overlapping. The images in the dataset are in gray level values.

For all experiments, a value of  $\alpha = 0$  and  $\beta = 10$  is used to control the smoothness of the curves in each patch. These curves are allowed to deform for 10 iterations. A value of  $\mu = 0.2$  is used for the regularization parameter to compute the GVF field, as suggested in [9]. The size of the patch is set to  $\tau = 10$ . The termination of the patch-based deformation is based on a value of  $\theta_L = 20^\circ$ .

The performance of the proposed framework is compared with state-of-the-art methods available from the literature. To the best of our knowledge, the methods presented in [2, 19] provide the best performance in the field of segmentation of overlapping cervical cells.

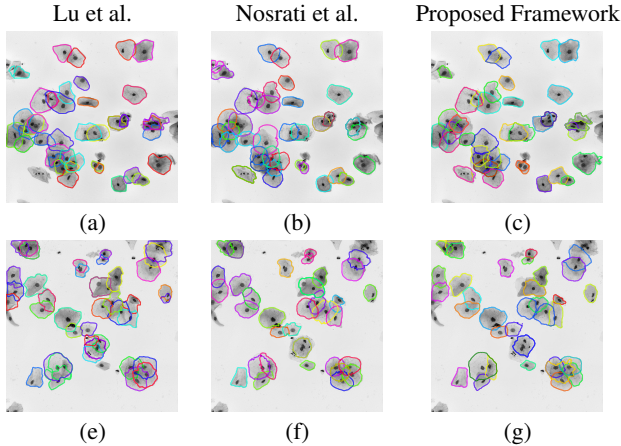


**Fig. 6.** Visual results of evaluated methods. The contours depicted in different colors show the detected cytoplasm boundaries.

The parameters of Nosrati et al.’s and Lu et al.’s methods are set to the values suggested in [2, 19].

The detection and segmentation accuracy on the tested EDF images is measured by the average Dice similarity coefficient (DSC) [24] over the *good* segmentations, using the provided ground truth. Here, we consider DSC values above 0.7 as *good* segmentation results [25]. Evaluations are performed on a total of 200 cells, which have an overlap coefficient in the range [0, 0.5]. Table 1 tabulates results of the evaluated methods and our framework. This table also tabulates the pixel-based evaluation using the true-positive (TP) rates and false-negative (FN) rates.

**Table 1.** Evaluation results for cytoplasm segmentation. Highlighted values represent the best results; values in parentheses represent the standard deviation. TP: true positive rates. FP: false positives rates.

Method	Dice (Pixel)	TP (Pixel)	FP (Pixel)
[19]	0.8600(0.0776)	0.8642(0.1023)	0.0011(0.0012)
[2]	0.8700(0.0900)	0.9000(0.1000)	0.0019(0.0016)
Proposed	<b>0.9140(0.0632)</b>	<b>0.9239(0.0711)</b>	<b>0.0008(0.0009)</b>

Visual results for Lu et al.’s method, Nosrati et al.’s method, and the proposed framework are shown in Fig. 6. Visual results of Lu et al.’s method show more detected cells in comparison to the other evaluated methods. This is mainly due to the good nucleus detection algorithm, which allows more cells to be correctly detected. However, this method fails to segment cells with a high degree of overlap. The method proposed by Nosrati et al. has advantages in the overlapping regions, regardless of the degree of overlap among cells. However, in terms of accuracy, this method is less precise in distinguishing the cells from the background because of the inaccurate random decision forest probability map used [2]. The results of the proposed framework confirm the quantitative results presented in Table 1.

In some cases where the cell has an oval shape rather than a circular shape, the method proposed by Lu et al. fails to accurately segment the cell. For instance, in clumps where there are two *oval* cells [see Fig. 7 (a)], Lu et al.’s method enforces the contour to be minimized in the overlapping area between the two cells. This is because the cytoplasm segmentation is underpinned by the initial contour, which is extrapolated using the boundaries of the cell clumps and the detected nuclei. If the contour is initialized in a region where two cytoplasm overlap, then it is likely to be minimized

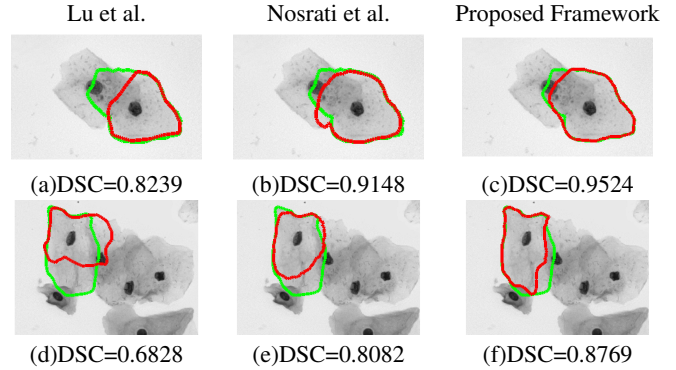


**Fig. 7.** Two examples of EDF cervical cytology image. Each row represents a case. The green contour denotes the ground truth, while the red contour denotes the results obtained by the corresponding method.

in the area between the two nuclei. The method proposed by Nosrati et al. provides more accurate results for this case [see Fig. 7 (b)] than those attained by Lu et al.’s method. This is mainly due to the elliptical-shape prior employed. Our proposed framework attains the most accurate result for this case [see Fig. 7 (c)]. This is mainly due to three important advantages of our the patch-based deformation. First, patch  $P_0$  is always initialized at one end of  $Cell_{overlap}$  [see points  $L_0$  and  $L_1$  in Fig. 3 (c)]. Second, the subsequent patches are initialized always in regions that represent the maximum region of the cell; this increases the likelihood of segmenting the whole cell. Third, the circular motion of the patches helps to detect a boundary that represents a more realistic cell shape.

The method proposed by Lu et al. also fails in cases where the cell nucleus is not exactly centred in the cell. This is mainly due to shape prior proposed by their method. Based on their observations that the majority of cytoplasm contours are located on pixels at the same relative distance from their associated nuclei, the shape prior is defined based on the geometry of the detected nuclei and clumps. This results in inaccurate segmentation results for the case depicted in Fig. 7 (d). Nosrati et al.’s method attains more accurate results than those attained by Lu et al.’s method in this case [see Fig. 7 (e)]. This is due again to the elliptical-shape prior employed. Because our proposed framework does not rely on a particular shape prior to deform the active contours, it provides more accurate results in this case [see Fig. 7 (f)]. In other words, our framework can segment a variety of cell shapes thanks to the patch-based deformation process.

#### 4. CONCLUSION

This paper presented a framework that addresses the problem of segmenting the cytoplasm of each individual cell in EDF images depicting overlapping cervical cells. The proposed framework uses a patch-based approach where a parametric active contour detects, on a patch-by-patch basis, the cytoplasm boundary of each overlapping cell. The active contour within each patch is deformed under the external influence of GVF forces computed based on local edge features collected from the patch region. Computing GVF forces on a patch-by-patch basis not only reduces computational costs, but also provides precise features, as computing these forces over the whole image may overlook small edge features. Experimental results showed that the proposed framework outperforms other state-of-the-art approaches, in terms of cytoplasm segmentation accuracy, as measured by the Dice similarity coefficient.

## 5. REFERENCES

- [1] W. H. O. R. Health, W. H. O. C. Diseases, and H. Promotion, *Comprehensive cervical cancer control: a guide to essential practice*. World Health Organization, 2006.
- [2] Z. Lu, G. Carneiro, and A. P. Bradley, "An improved joint optimization of multiple level set functions for the segmentation of overlapping cervical cells," *IEEE Transactions on Image Processing*, vol. 24, no. 4, pp. 1261–1272, 2015.
- [3] H. Z. Noorani, C. Arratoon, A. Hall, C. C. O. for Health Technology Assessment *et al.*, *Assessment of techniques for cervical cancer screening*, 1997.
- [4] I. Dagher and K. El Tom, "Waterballoons: A hybrid watershed balloon snake segmentation," *Image and Vision Computing*, vol. 26, no. 7, pp. 905–912, 2008.
- [5] E. Bengtsson, "Recognizing signs of malignancy: the quest for computer assisted cancer screening and diagnosis systems," in *Computational Intelligence and Computing Research (ICCIC), 2010 IEEE International Conference on*. IEEE, 2010, pp. 1–6.
- [6] E. Bengtsson, "Computerized cell image analysis: past, present, and future," in *Scandinavian Conference on Image Analysis*. Springer, 2003, pp. 395–407.
- [7] A. Khadidos, V. Sanchez, and C.-T. Li, "Active contours based on weighted gradient vector flow and balloon forces for medical image segmentation," in *Proceedings of International Conference on Image Processing (ICIP)*. IEEE, 2014, pp. 902–906.
- [8] A. Khadidos, V. Sanchez, and C.-T. Li, "Active contours with weighted external forces for medical image segmentation," in *Proceedings of Medical Image Understanding and Analysis (MIUA)*, 2014, pp. 149–154.
- [9] C. Xu and J. L. Prince, "Snakes, shapes, and gradient vector flow," *IEEE Transactions on Image Processing*, vol. 7, no. 3, pp. 359–369, 1998.
- [10] C. Jung, C. Kim, S. W. Chae, and S. Oh, "Unsupervised segmentation of overlapped nuclei using bayesian classification," *IEEE Transactions on Biomedical Engineering*, vol. 57, no. 12, pp. 2825–2832, 2010.
- [11] A. Kale and S. Aksoy, "Segmentation of cervical cell images," in *International Conference on Pattern Recognition (ICPR)*. IEEE, 2010, pp. 2399–2402.
- [12] K. Li, Z. Lu, W. Liu, and J. Yin, "Cytoplasm and nucleus segmentation in cervical smear images using radiating gvf snake," *Pattern Recognition*, vol. 45, no. 4, pp. 1255–1264, 2012.
- [13] M. E. Plissiti, C. Nikou, and A. Charchanti, "Automated detection of cell nuclei in pap smear images using morphological reconstruction and clustering," *IEEE Transactions on Information Technology in Biomedicine*, vol. 15, no. 2, pp. 233–241, 2011.
- [14] S.-F. Yang-Mao, Y.-K. Chan, and Y.-P. Chu, "Edge enhancement nucleus and cytoplasm contour detector of cervical smear images," *IEEE Transactions on Systems, Man, and Cybernetics, Part B: Cybernetics*, vol. 38, no. 2, pp. 353–366, 2008.
- [15] M. E. Plissiti, C. Nikou, and A. Charchanti, "Combining shape, texture and intensity features for cell nuclei extraction in pap smear images," *Pattern Recognition Letters*, vol. 32, no. 6, pp. 838–853, 2011.
- [16] Y. Marinakis, G. Dounias, and J. Jantzen, "Pap smear diagnosis using a hybrid intelligent scheme focusing on genetic algorithm based feature selection and nearest neighbor classification," *Computers in Biology and Medicine*, vol. 39, no. 1, pp. 69–78, 2009.
- [17] Z. Lu, G. Carneiro, and A. P. Bradley, "Automated nucleus and cytoplasm segmentation of overlapping cervical cells," in *Medical Image Computing and Computer-Assisted Intervention (MICCAI)*. Springer, 2013, pp. 452–460.
- [18] M. S. Nosrati and G. Hamarneh, "Segmentation of overlapping cervical cells: a variational method with star-shape prior," in *IEEE 12th International Symposium on Biomedical Imaging (ISBI)*. IEEE, 2015, pp. 186–189.
- [19] M. Nosrati and G. Hamarneh, "A variational approach for overlapping cell segmentation," *ISBI Overlapping Cervical Cytology Image Segmentation Challenge*, pp. 1–2, 2014.
- [20] A. P. Bradley and P. C. Bamford, "A one-pass extended depth of field algorithm based on the over-complete discrete wavelet transform," in *Image and Vision Computing'04 New Zealand (IVCNZ'04)*. not found, 2004, pp. 279–284.
- [21] J. Matas, O. Chum, M. Urban, and T. Pajdla, "Robust wide-baseline stereo from maximally stable extremal regions," *Image and vision computing*, vol. 22, no. 10, pp. 761–767, 2004.
- [22] A. Vedaldi and S. Soatto, "Quick shift and kernel methods for mode seeking," in *Computer vision—ECCV 2008*. Springer, 2008, pp. 705–718.
- [23] W. A. Barrett and E. N. Mortensen, "Interactive live-wire boundary extraction," *Medical image analysis*, vol. 1, no. 4, pp. 331–341, 1997.
- [24] L. R. Dice, "Measures of the amount of ecologic association between species," *Ecology*, vol. 26, no. 3, pp. 297–302, 1945.
- [25] P. Radau, Y. Lu, K. Connelly, G. Paul, A. Dick, and G. Wright, "Evaluation framework for algorithms segmenting short axis cardiac mri," *The MIDAS Journal*, vol. 49, no. 6, 2009.